Joint Centre for Mesoscale Meteorology, Reading, UK

Investigation of Different Representations of Rain in a 1-D Evaporation Model

H. Swann

Internal Report No. 59

May 1996

Met Office Joint Centre for Mesoscale Meteorology Department of Meteorology
University of Reading PO Box 243 Reading RG6 6BB United Kingdom
Tel: +44 (0)118 931 8425 Fax: +44 (0)118 931 8791
www.metoffice.com

Designed and produced by the Met Office © Crown copyright 2001 01/0240 The Met Office logo is a registered trademark.

INVESTIGATION OF DIFFERENT REPRESENTATIONS OF RAIN IN A 1–D EVAPORATION MODEL

Hugh Swann

1 Introduction

The bulk–microphysics scheme previously used in the U.K. Met. Office Large Eddy Model has single–moment bulk–water representation of precipitating particles, in common with most other cloud resolving models, (eg. Flatau *et al.* 1989, Lin *et al.* 1983). In such schemes, precipitating particles are represented by just one variable (**q**, the mass–mixing ratio) so the number concentration and the mean drop diameter both increase monotonically as a function of **q**. More recently, however, a double–moment bulk–water scheme heas been implaemnted, which uses two variables to represent precipitating particles (the mass–mixing ratio and **n**, the particle number concentration). This reduces the number of adjustable coefficients and allows some processes to be modelled in a more realistic way than is possible with the simpler schemes because the number concentration (and hence the mean diameter) is allowed to vary independently of the mass–mixing ratio.

One feature of cloud simulations that the double–moment scheme is expected to model more accurately is the reduction of the number of small drops compared to larger drops in the evaporation region of rain. The single–moment schemes, especially when an exponential drop size distribution is assumed, implies generation of small drops at a rate faster than they would be generated through the evaporation of large drops, as found by Clough and Franks (1991). A simple 1–D evaporation model with a 'passive' atmosphere is used to model rain falling through subsaturated air to the surface, causing rainfall rates of up to 10mm/h.

Three different representations of rain are compared, a single–moment scheme, a double–moment scheme and an explicit scheme. The shape of the initial drop size distribution is assumed to be either an exponential or a generalised gamma distribution (the explicit scheme is able to deviate from this initial shape, whereas the bulk water schemes can not). The explicit scheme uses a large number of variables each representing a size bin of rain drops. This method is too computa-

tionally expensive to be used in a 3–D model, but can be used in this 1–D model to produce an exact solution to the precipitation and evaporating equations, for evaluating the bulk–water approximations.

2 Description of the 1–D model

The 1–D model represents an evaporating layer below a presipitating cloud. The model can be initiated with either a parcel of rain near the top of its domain or with a constant flux of rain through the top boundary. Initial values of **n** and **q** are chosen so that the rain drop size spectrum is initially identical in the three schemes. The model is then integrated in time so the rain precipitates down through the domain, until either all the rain has reached the ground (in the rain parcel experiments) or until a steady state has been reached (in the constant flux experiments). Evaporation in the model can be switched on or off, so the effect of precipitation alone can be analysed (large drops fall faster than smaller drops, which affects the shape of the drop size spectra). The evolution of the spatial distribution of rain and the drop size–spectra is diagnosed at intervals through the integration for the three schemes, single–moment, double–moment and explicit.

The purpose of this study is to compare the two bulk schemes and to validate them against the explicit scheme. No attempt has been made to model a real case and validate against observations, as a 3–D cloud model is more appropriate for this purpose, as described in Section 6. Thus the 1-D model has a 'passive' atmosphere, *ie.* the temperature and humidity profiles have no response to the evaporation.

2.1 Single–Moment Representation

This representation of rain uses just one model variable, the rain mass mixing ratio (**q**). The shape of the size spectra and the number concentration of drops is diagnosed from this one variable and a number of adjustable coefficients. The number of drops of each size is given by a gamma distribution:

$$n(D) = n_0 D^{\alpha} e^{-\lambda D} \tag{1}$$

where n_0 and α are constants. Given that the mass–diameter relationship is $M(D) = cD^d$ (with $c = 523.9\text{kgm}^{-3}$ and $d = 3$), the slope function, λ, can be determined as a function of $\mathbf{q}$,

$$\lambda = \left(\frac{n_0 c\Gamma(1+\alpha+d)}{\rho \mathbf{q}}\right)^{\frac{1}{1+\alpha+d}}. \tag{2}$$

The number concentration mixing ratio (ie number of drops per kg of air) can also be diagnosed:

$$n = \frac{\Gamma(1+\alpha)n_0}{\rho\lambda^{1+\alpha}}. \tag{3}$$

The prognostic equation for this bulk variable is

$$\frac{d\mathbf{q}}{dt} = \frac{1}{\rho}\frac{\partial}{\partial z}(\rho \mathbf{q}[V]_q) + P_{REVP}, \tag{4}$$

where $[V]_q$ is the mass-mean fall velocity and P_{REVP} is the bulk conversion rate of rain to vapour due to evaporation, given by equations (12) and (16) respectively.

2.2 Double–Moment Representation

This representation of rain uses two model variables, the rain mass mixing ratio ($\mathbf{q}$) and the number concentration mixing ratio ($\mathbf{n}$). A gamma distribution of particle sizes is assumed, as for the single–moment scheme, but the spectrum isn't limited by the assumption of a constant intercept parameter. Equations (3) and (2) all still valid for this scheme, but are more useful if rearranged because the intercept parameter, n_0 is no longer a constant, but a function of $\mathbf{q}$ and $\mathbf{n}$. As a function of the two model variables, the slope and intercept parameters are,

$$\lambda = \left(\frac{\mathbf{n}c\Gamma(1+\alpha+d)}{\mathbf{q}\Gamma(1+\alpha)}\right)^{\frac{1}{d}}, \tag{5}$$

$$n_0 = \frac{\rho \mathbf{n}\lambda^{1+\alpha}}{\Gamma(1+\alpha)}. \tag{6}$$

The prognostic equation for the two bulk variables are

$$\frac{d\mathbf{q}}{dt} = \frac{1}{\rho}\frac{\partial}{\partial z}(\rho \mathbf{q}[V]_q) + P_{REVP}, \tag{7}$$

$$\frac{d\mathbf{n}}{dt} = \frac{1}{\rho}\frac{\partial}{\partial z}(\rho \mathbf{n}[V]_n) + R_{REVP}, \tag{8}$$

where $[V]_n$ is the number-mean fall velocity and R_{REVP} is the drop concentration depletion due to evaporation.

2.3 Explicit Representation

This scheme divides the rain into N size bins N=20 for the simulations described). The mass mixing ratio of rain in each diameter range is $\mathbf{q_i}$, so that the total mass mixing ratio is given as

$$q = \sum_{i=1}^{N} \mathbf{q_i}. \tag{9}$$

The diameters represented by each bin are spaced logarithmically between a maximum and a minimum diameter, so the diameter of drops in the i^{th} category is

$$D_i = D_{min} e^{\frac{i}{N}(ln(D_{max}) - ln(D_{min}))} \tag{10}$$

where D_{min}=0.02mm and D_{max}=8mm.

The prognostic equation for each size category is

$$\frac{d\mathbf{q_i}}{dt} = \frac{1}{\rho}\frac{\partial}{\partial z}(\rho \mathbf{q_i}[V]_i) + P_{REVPi}, \tag{11}$$

where $[V]_i$ is the fall velocity of drops of diameter D_i, given by equation (14) and P_{REVPi} is the rate change of mass in the i^{th} category due to evaporation, given by equation(19)

2.4 Fall speed

For both of the bulk schemes the rain is advected downward according its the mass mean fall speed. The generalised fall speed – diameter relationship for a drop is $V(D) = aD^b e^{-fD}\left(\frac{\rho_0}{\rho}\right)^{0.5}$, where a, b and f are constant coefficients, ρ is the air density and the reference air density, $\rho_0 = 1.22\text{kgm}^{-3}$. Values of constants used in this study are a=4854s^{-1}, b=1 and f=1.95 following Uplinger (1981).

So the mass mean fall speed is

$$\begin{aligned}[V]_q &= \frac{\int M(D)n(D)V(D)dD}{\rho \mathbf{q}} \\ &= a\frac{\Gamma(1+\alpha+d+b)\lambda^{1+\alpha+d}}{\Gamma(1+\alpha+d)(\lambda+f)^{1+\alpha+d+b}}\left(\frac{\rho_0}{\rho}\right)^{0.5}.\end{aligned} \tag{12}$$

For the double–moment scheme, the fall speed for the rain number concentration is advected downward at the mean fall speed, weighted by number concentration,

$$\begin{aligned}[V]_n &= \frac{\int n(D)V(D)dD}{\rho \mathbf{n}} \\ &= a\frac{\Gamma(1+\alpha+b)\lambda^{1+\alpha}}{\Gamma(1+\alpha)(\lambda+f)^{1+\alpha+b}}\left(\frac{\rho_0}{\rho}\right)^{0.5} \end{aligned} \tag{13}$$

The downward advection in the explicit scheme is simple; all drops in each size category will fall at the same velocity. So

$$[V]_i = aD_i^b e^{-fD_i}\left(\frac{\rho_0}{\rho}\right)^{0.5}. \tag{14}$$

2.5 Evaporation

The rate of change of mass of a rain drop due to evaporation based on Byers (1965) is

$$\frac{dM}{dt} = \frac{2\pi D\left(\frac{q_v}{q_{sat}}-1\right)}{A'+B'}F' \tag{15}$$

where q_{sat} is the saturation mixing ratio, q_v is the vapour mixing ratio, A' and B' are thermodynamic coefficients, $A' = \frac{L_v^2}{K_a R_w T^2}$ and $B' = \frac{1}{\rho q_{sat}\psi}$ and F' is the ventilation factor which is given by Thorpe and Mason (1966) as $F' = 0.78 + 0.31 S_c^{\frac{1}{3}} R_e^{\frac{1}{2}}$ where the Reynolds number, $R_e = V(D)D\rho/\upsilon$ and the Schmidt number, $S_c = \upsilon/\psi$. $\upsilon = 1.44\times10^{-5}\mathrm{m}^2\ \mathrm{s}^{-1}$ is the kinematic viscosity of air and ψ=$2.26\times10^{-5}\mathrm{m}^2\ \mathrm{s}^{-1}$ is the diffusivity of water vapour in air.

When integrated over all diameters this gives the bulk conversion rate from rain to vapour due to evaporation,

$$P_{REVP} = \frac{2\pi\left(\frac{q_v}{q_{sat}}-1\right)}{\rho(A'+B')}n_{0R}$$

$$\times\left[0.78\lambda^{-(2+\alpha)} + 0.31 S_c^{\frac{1}{3}}\Gamma\left(\alpha+\frac{b+5}{2}\right)a^{0.5}\upsilon^{-0.5}(\rho_0\rho)^{0.25}\right.$$

$$(\lambda + 0.5f)^{-\left(\alpha+\frac{b+5}{2}\right)}\Big]. \tag{16}$$

The change of number concentration in the double-moment scheme is calculated using a simple parametrisation that assumes that the mean mass of the particles that are 'lost' due to evaporation is equal to the number-mean mass of the rain drops, this agrees well with the explicit scheme and is used by Ferrier (1993). So the sink term for n is,

$$R_{REVP} = \frac{\mathrm{n}}{\mathrm{q}} P_{REVP}. \tag{17}$$

In the explicit scheme the rate of loss of mass due to evaporation from the i^{th} size category is,

$$\left(\frac{\partial q_i}{\partial t}\right)_{evap} = \frac{\mathrm{q_i}}{cD_i^d} \frac{2\pi\left(\frac{q_v}{q_{sat}} - 1\right)}{(A' + B')}$$

$$\times \left[0.78D_i + 0.31S_c^{\frac{1}{3}} a^{0.5} \upsilon^{-0.5} (\rho_0\rho)^{0.25} D_i^{\frac{b+3}{2}} e^{-0.5fD_i}\right]. \tag{18}$$

As the particles evaporate from the i^{th} category they move down to the $(i-1)^{th}$ category, conserving the number of particles. The number of particles required to shift down one size category to cause this mass reduction is $\frac{1}{M_i - M_{i-1}}\left(\frac{\partial \mathrm{q_i}}{\partial t}\right)_{evap}$ so the source term for each $\mathrm{q_i}$ is

$$P_{REVPi} = \frac{M_i}{M_{i+1} - M_i}\left(\frac{\partial \mathrm{q_{i+1}}}{\partial t}\right)_{evap} - \frac{M_i}{M_i - M_{i-1}}\left(\frac{\partial \mathrm{q_i}}{\partial t}\right)_{evap}. \tag{19}$$

The particles in the smallest size category q_1 are assumed to completely evaporate every timestep.

3 Simulations without evaporation

Two simulations were carried out which allowed the rain to fall without evaporating. The effect that precipitation has on the size spectrum can then be considered in isolation. The model is initiated with a parcel of rain at 1800m, and diagnostics of rain amount and mean diameter are plotted at intervals as the rain precipitates to the surface, causing a rainfall rate at the ground of up to 6mm/h. As large drops fall faster than small drops, the drop size spectrum will alter with height and with time. This effect can be modelled accurately with the explicit scheme and the bulk parametrizations can be compared to this result.

In *run 1* the intercept parameter, used to initialise the size spectra and is held constant for the single–moment scheme, is set as $n_0 = 8 \times 10^6 m^{-4}$ and the gamma distribution shape parameter is $\alpha = 0$, giving an exponential size spectra, based on Kessler (1969). The tables and profile plots in figure 1 show a number of discrepancies between the explicit scheme and the bulk schemes.

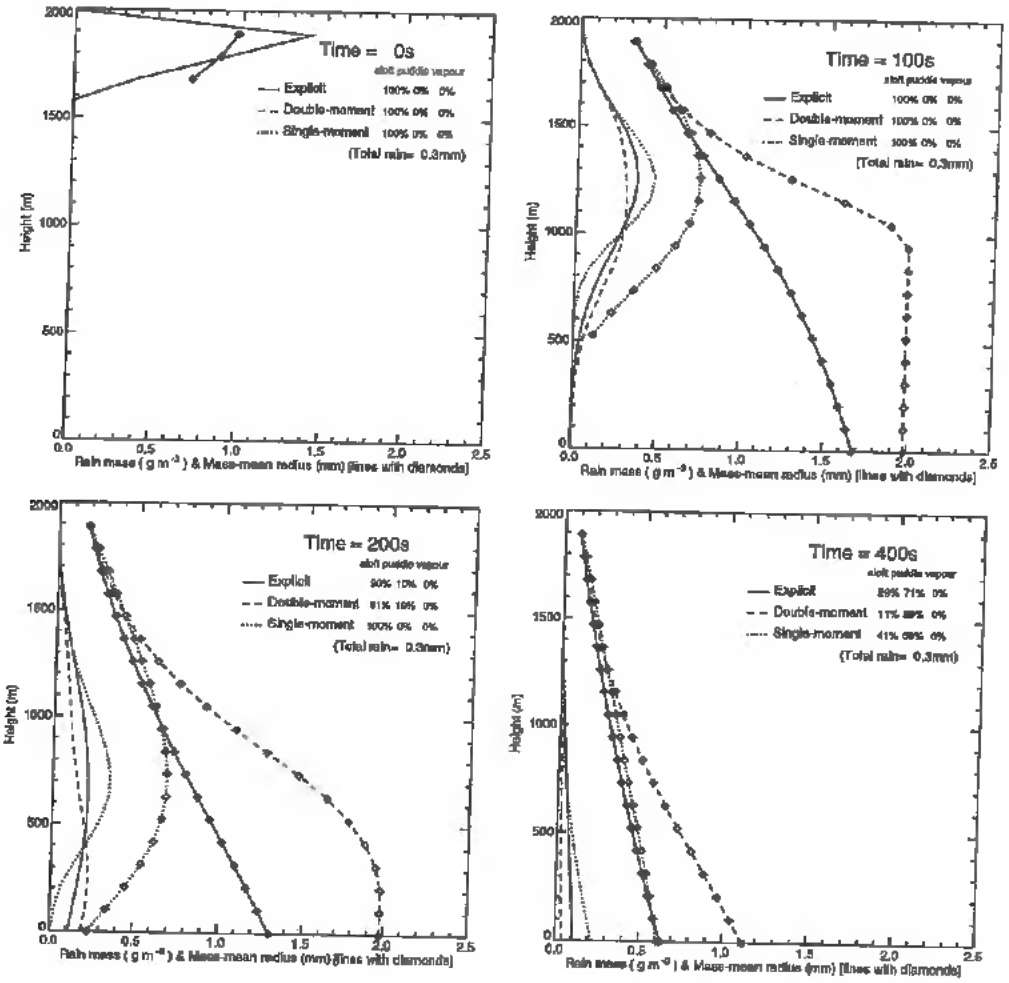

Figure 1: *Mass mixing ratios and radius profiles evolving with time for* run 1 *where* $\alpha = 0$ *and initially* $n_0 = 8 \times 10^6 m^{-4}$. *There is no evaporation in this simulation.*

The single–moment scheme underestimates the mean radius, so the rain falls too slowly so that by 400s only 59% of the rain has reached the surface, compared to 71% for the explicit scheme. This is because the mean diameter and hence the fall speed is underestimated by this scheme. The drop number concentration is a function of q when using single–moment representation and the total number of drops is not conserved. The total drop number is initially 10^6 m^{-2} for all

three schemes but after 100 seconds of integration this quantity is diagnosed to be 3×10^6 m^{-2} in the single–moment scheme whereas it should be conserved.

The double–moment scheme correctly models an increase of mean radius below the initial parcel of rain, caused by the larger drops falling faster, though this effect though is over estimated. The mass mean radius is far larger than that modelled by the explicit scheme. The reason for this is the widening of the drop size spectrum, caused by assuming an exponential distribution of sizes. The upper limit to the mean radius, as can be seen on the plots, is imposed by increasing $\mathbf{n}$, but this is an unsatisfactory (and unphysical) way of remedying the problem. This source of particles increases the total drop number by around 5% in this simulation.

In *run 2* a non-zero value of the shape parameter was used, resulting in a sharper distribution of drop sizes. A smaller proportion of drops are significantly larger than the mean drop size which should reduce the broadening of the drop size distribution producing unrealistically large drops in the air below the initial parcel of rain, as occurred in the double–moment scheme in *run 1*. The value chosen for the shape parameter was $\alpha = 2.5$ as derived from optical spectrometer measurements by Willis (1984) which is held constant for both of the bulk schemes. The intercept parameter was $n_0 = 1.21 \times 10^{15}m^{-1.5}$ which is used to initialise the drop spectra for all the schemes, and is held constant in the single–moment scheme. This value of n_0 was chosen because it gives the same initial mass-mean fall speed as in *run 1*.

In *run 2* (as can be seen in the plots in figure 2 the rain profile modelled by the double–moment scheme follows that of the explicit scheme more closely than in *run 1* and more closely than the single–moment scheme is able to do. An upper limit to the mean radius is imposed , but over a smaller portion and for less time than in *run 1*. The increase in $\mathbf{n}$ required to limit the mean mass radius to 2mm was only 1%.

4 Simulations with evaporation

The same 'falling rain parcel' simulations were repeated, but with evaporation switched on. A constant relative humidity of 60% was assumed throughout the domain, and a surface temperature of 17°C, falling to –3°C at a height of 2000m.

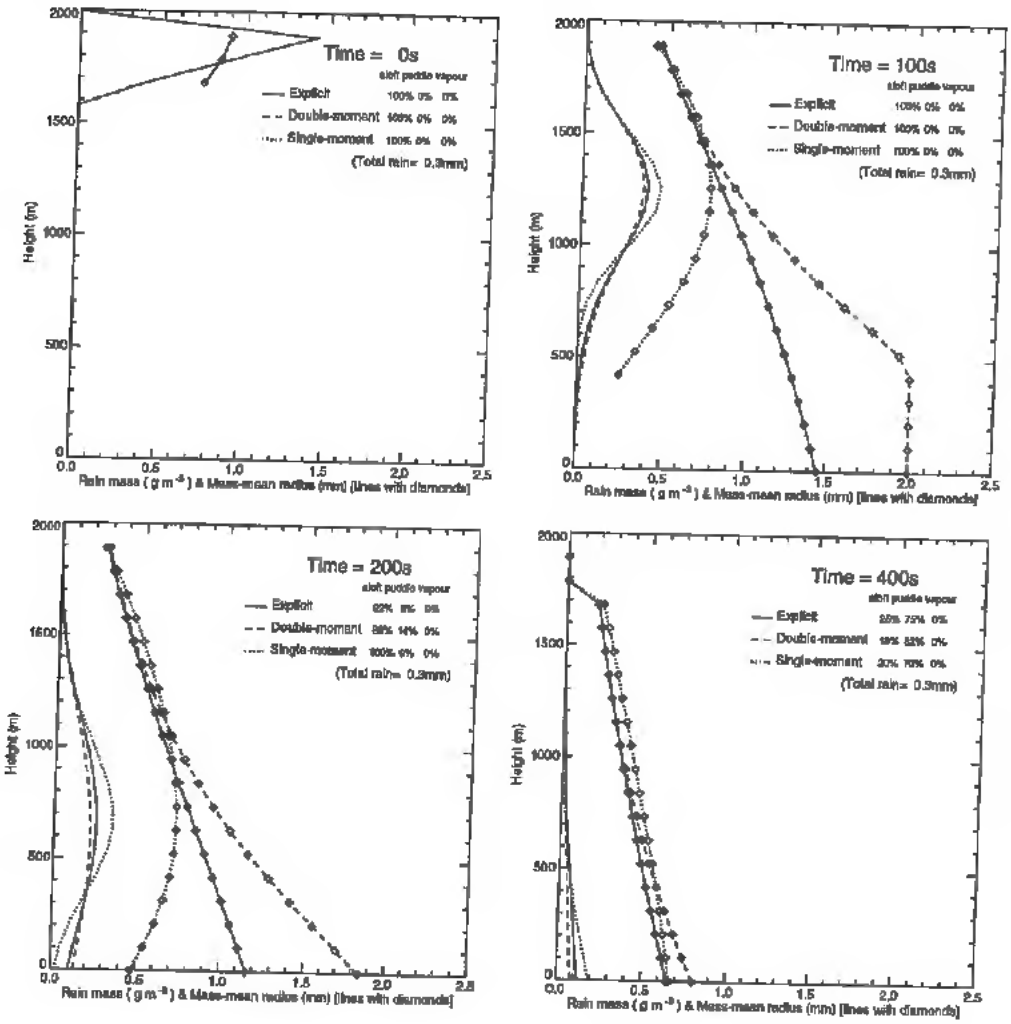

Figure 2: *Mass mixing ratios and radius profiles evolving with time for* run 2 *where* $\alpha = 2.5$ *and initially* $n_0 = 1.21 \times 10^{15} m^{-1.5}$. *There is no evaporation in this simulation.*

Run 3 (illustrated in figure 3) has the same drop spectra approximations as *run 1* and *Run 4* (illustrated in figure 4) has the same drop spectra approximations as *run 2*.

In figure 3 it can be seen that the single–moment scheme causes too much of the rain to be evaporated. This is because the constant intercept parameter approximation underestimates the mean diameter, as discussed in the previous section. All the rain, as described by the single–moment scheme, has evaporated after 400 seconds of intergration, compared to 63% using the explicit scheme. The double–moment scheme, although it overestimates the mean radius, especially near the ground, is an improvement over the single–moment scheme. After 400

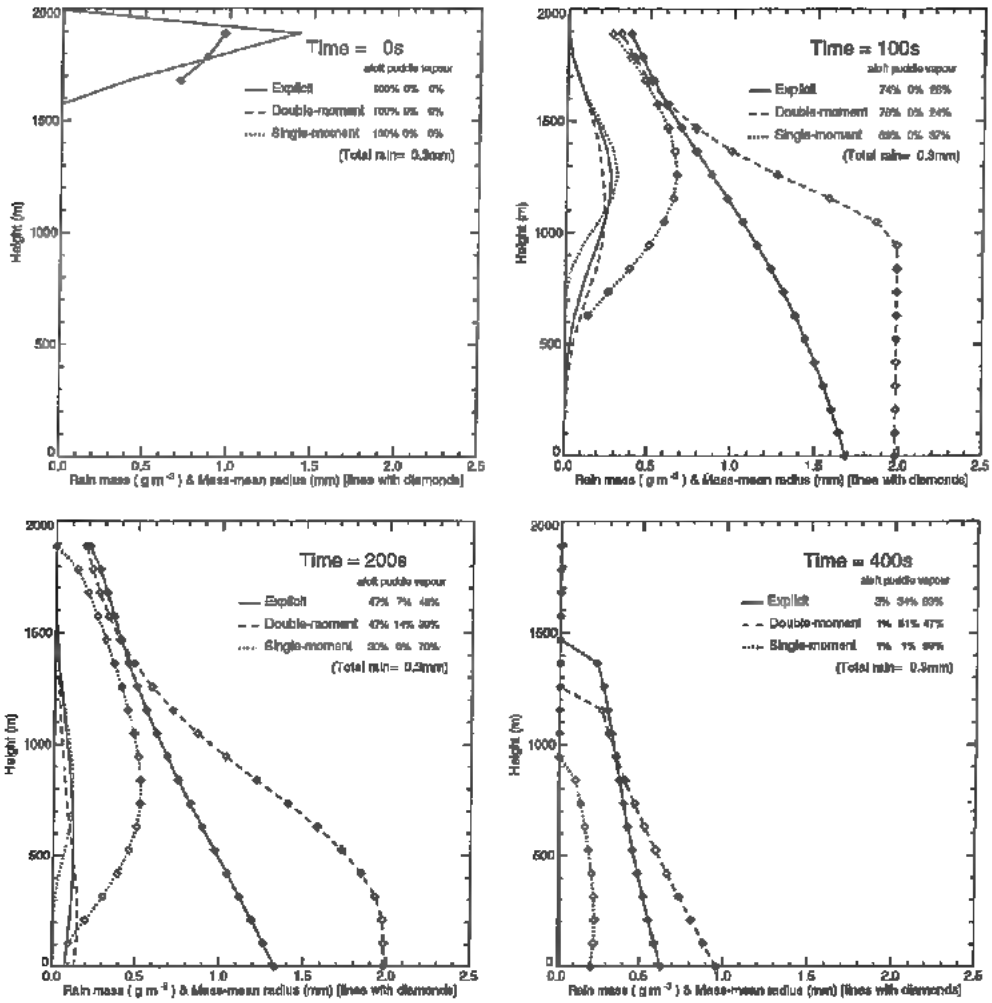

Figure 3: *Mass mixing ratios and radius profiles evolving with time for* run 3 *where* $\alpha = 0$ *and initially* $n_0 = 8 \times 10^6 m^{-4}$. *Evaporation is switched on in this simulation.*

seconds, 48% of the initial rain has evaporated.

The final 'falling rain parcel' experiment, *run 4* has the shape parameter set to $\alpha = 2.5$. Both the bulk schemes agree more closely with the explicit scheme than in *run 3* (see figure 4). With this value of the shape parameter, giving less variance of rain drop sizes, the single–moment scheme assumes that a smaller proportion of the rain drops are of very small radius, so the amount of evaporation is less than in *run 3*. The double–moment representation is improved because the concentration of large drops is not artificially increased due to the assumption of a broad size spectrum. By the end of the simulation, the single–moment scheme has over predicted the amount of evaporation by 19% and the double–moment

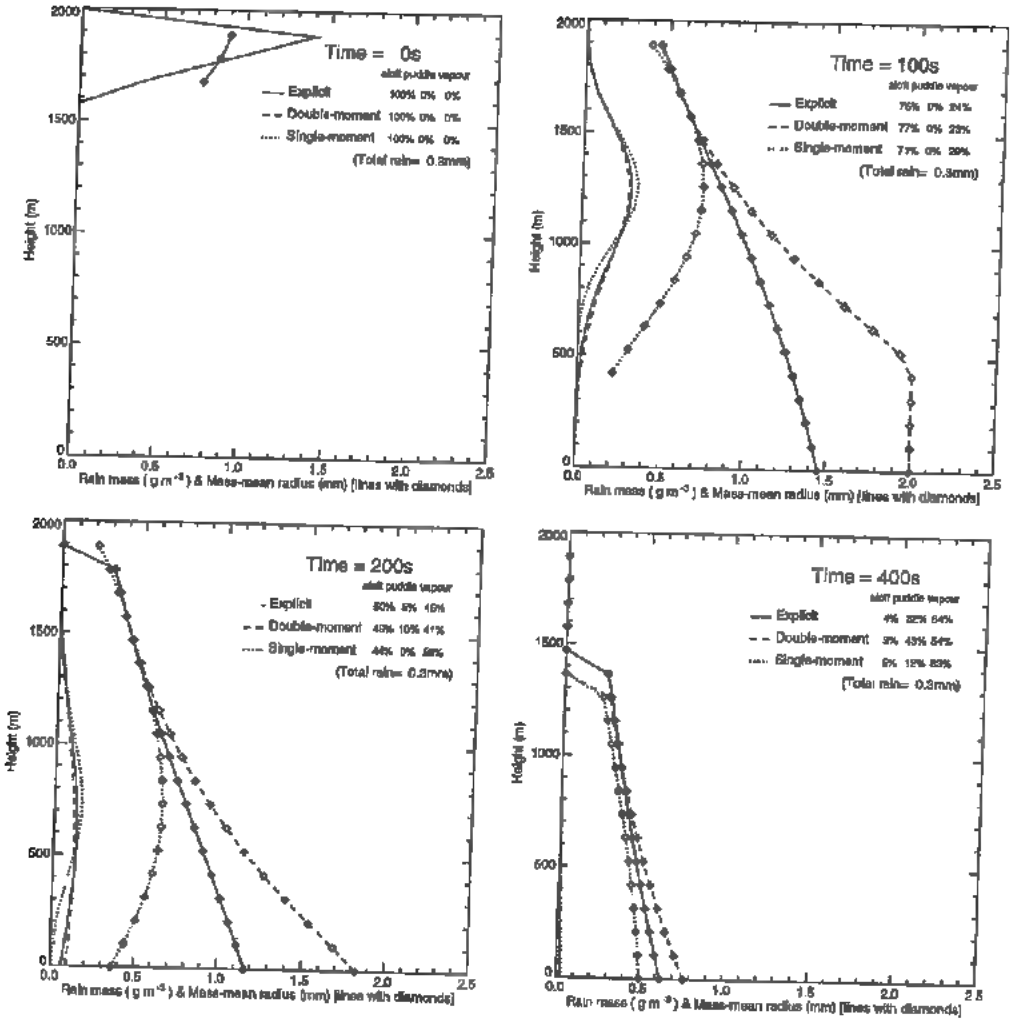

Figure 4: *Mass mixing ratios and radius profiles evolving with time for* run 4 *where* $\alpha = 2.5$ *and initially* $n_0 = 1.21 \times 10^{15} m^{-1.5}$. *Evaporation is switched on in this simulation.*

scheme has under-predicted evaporation by just 10%.

The change in relative humidity of the environmental air, which has been neglected for this experiment, would be small small. The increases in relative humidity caused by the evaporation of rain would be in the range of 3 to 4%, giving final RH of between 63% and 64%.

5 Constant Flux Simulations

These simulations have a constant flux of rain into the top of the domain at a height of 2km. The simulations can be run to a steady state since the humidity is held at a constant 60% so the moistening of the domain is neglected. The rates of evaporation and surface precipitation can be compared in the three schemes. The size spectrum of rain drops is the same for the three schemes at the upper boundary of the domain but is allowed to change with height as predicted by the individual schemes. The mass mean drop radius is plotted alongside the rain mass concentration in figures 5 and 6 to indicate how the rain drop spectra have evolved. The spectra can be seen in more detail in the plots on the right of the figures showing how mass is distributed amoung the different drop sizes for each of the different schemes at heights of 2000m, 1000m and at the ground.

In *run 5* a constant flux of rain of 22.1 mm h^{-1} enters the top of the domain. The results in figure 5 show the steady state profiles after 1200s of integration, and also the rainfall rate at the surface and the rate that rain is evaporating for each of the three schemes. It can be seen that the explicit scheme shows that the mass mean rain drop radius is larger nearer the ground. This is due to the depletion of smaller drops due to them evaporating faster than the larger drops. The double moment scheme also shows larger drops near the surface, but the single–moment scheme (which assumes that the mean radius is a function of mixing ratio) has the drops smaller near the surface. The double–moment scheme is close to the explicit scheme in predicting the rate at which rain falls to the ground and is evaporated, the results differing by 10%. The over-estimate of the rainfall rate by the double–moment scheme is due to the artificial broadening of the size spectrum causing the number of large drop to be overestimated, as can be seen in the plot of mass distribution (Figure 5), bottom right).

The single–moment scheme over estimated the amount of evaporation due to its underprediction of drop radius. The rain reaching the ground is 55% lower than that modelled by the explicit model, predicting a rainfall rate of 4.3mm/h as opposed to 9.5mm/h.

Run 6 is identical to *run 5* except that the shape parameter is set to $\alpha = 2.5$, giving a sharper shaped size spectrum (as in *run 2* and *run 4*). The shape parameter and intercept parameter are used to initialise the size spectra for all three schemes. The shape parameter is held constant for both the bulk schemes whereas the intercept parameter is held constant for only the single–moment

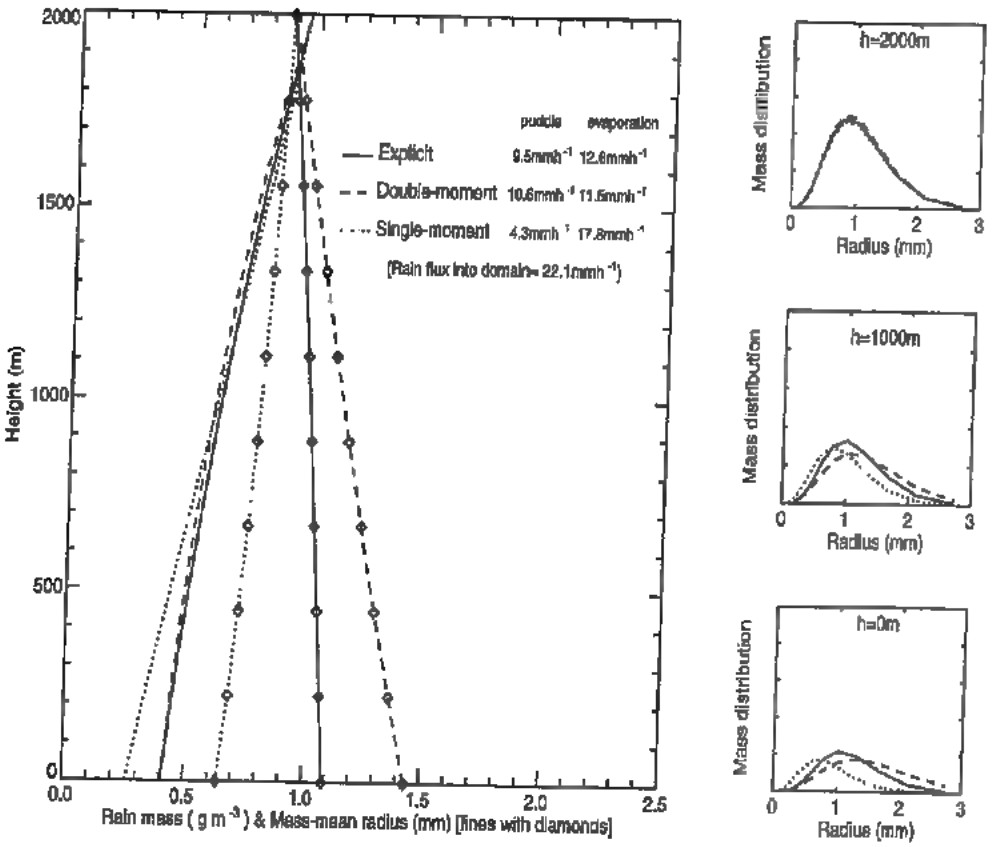

Figure 5: *Steady state mixing ratios and radius profiles for* run 5, *assuming a constant flux of rain into the top of the domain. Initially* $\underline{\alpha = 0}$ *and* $n_0 = 8 \times 10^6 m^{-4}$. *On the right are plots of the mass distribution amoung different drop sizes at the top, the middle and the bottom of the column. Evaporation is switched on in this simulation.*

scheme. The value of the intercept parameter ($n_0 = 1.21 \times 10^{15} \mathrm{m}^{-1\,5}$) was chosen so that mass mean fall velocity at the upper boundary equals that given by an exponential size distribution, as in *run 5*.

As in *run 4* this change in the shape parameter has lead to an improvement in both the single–moment and the the double–moment bulk schemes when validated against the explicit scheme. The single–moment scheme overestimates the evaporation by 16%, this discepency is due to the scheme assuming too small a radius. The double–moment scheme predicts the evaporation extremely accuratly, underestimating it by only 4%. The difference between the double–moment and explicit scheme is that the double–moment scheme slightly overestimates of the number of very large drops (over 1.5mm radius). This broadening of the spectrum in the double–moment scheme is not as pronounced as in *run 5*.

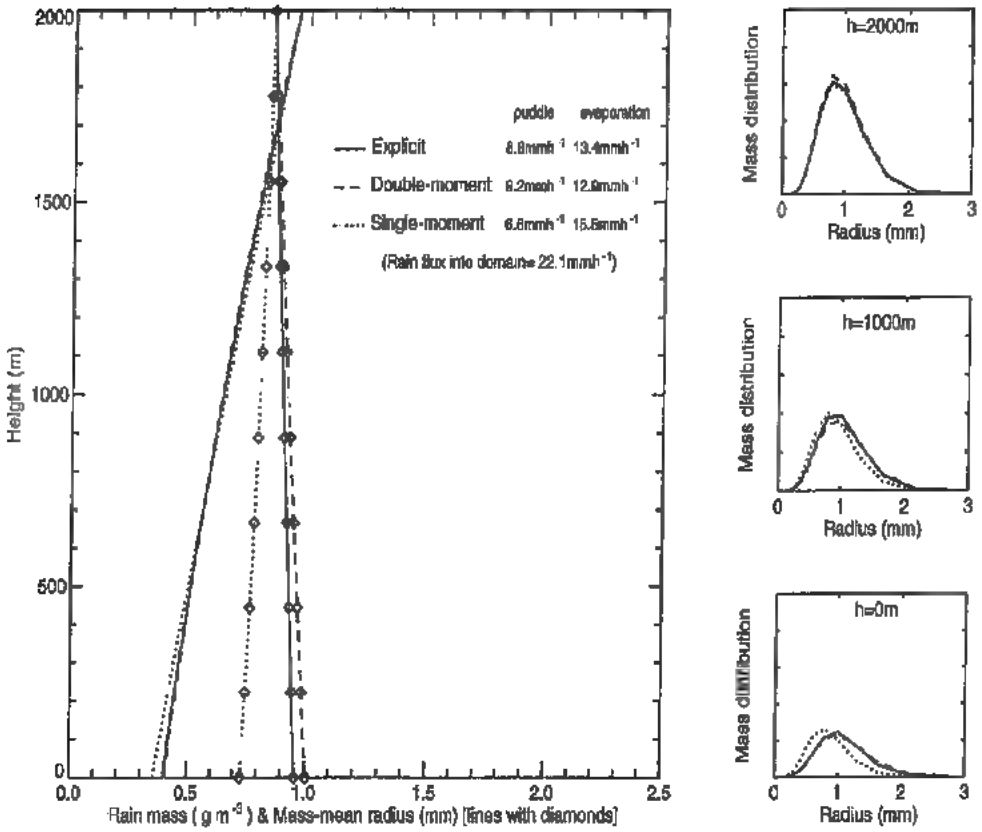

Figure 6: *Steady state mixing ratios and radius profiles for* run 6, *assuming a constant flux of rain through the top of the domain. Initially* $\underline{\alpha = 2.5}$ *and* $n_0 = 1.21 \times 10^{15} m^{-1.5}$. *On the right are plots of the mass distribution amoung different drop sizes at the top, the middle and the bottom of the column. Evaporation is switched on in this simulation.*

6 Use of non-zero α_R in a 3-D simulation.

Two simulations were carried out of showers over southern England, observed by the Chilbolton radar on March 17^{th}, 1991. A model grid of 30km × 30km × 12km was used with 500m resolution in the horizontal and up to 300m resolution in the vertical. The simulation is initialised with the temperature and humidity profile recorded by the midday radiosonde ascent at Crawley and a large number of small random heat perturbations near the surface were included to represent surface inhomogeneities that initiate convection.

The microphysics was modelled using an eight-variable scheme, with variables representing the mass-mixing ratios of liquid cloud+vapour, rain, snow, ice cloud

and graupel. Three further variables are used for the double–moment representation of the precipitating ice particles, so the number concentration of ice cloud, snow and graupel is predicted. The rain, however, is modelled using only single–moment representation, so the number concentration and mean drop diameter *etc.* are diagnosed from just the mass-mixing ratio, using an assumption of a generalised gamma distribution of drop sizes. Double-moment representation of rain has not been implemented because this would introduce the problem of parametrizing drop break–up and coalescence (as discussed in Section 7), these processes can be neglected for the ice precipitating particles, as ice crystals, snow and graupel do not break–up and coalesce as readily as liquid drops.

The case was first modelled assuming an exponential size spectrum for rain drops, ie. the shape parameter, α_R=0 . In regions away from the heaviest precipitation, where light rain is formed by the melting of snow, the model was found to over predict the evaporation rate of rain. This over–prediction of evaporation has been noted in simulations of other case studies, Brown and Swann (1996). The second simulation assumes a generalised gamma-distribution of rain drop sizes, with the shape parameter, α_R=2.5. The 1-D model results show that this assumption should reduce the evaporation rate, especially where the rain is light.

At 80 minutes into the simulations, cross–sections are plotted from a vertical slice through the most active convective cell in the model domain. These plots show the rain, snow, graupel and liquid cloud amounts as well as the diagnosed radar reflectivity for the two model simulations, with α_R -0 in figure 7 (top row) and α_R=2.5 in figure 7 bottom row).

It can be seen that the light rain away from the cell core penetrates all the way to the surface in the run with α_R = 2.5, producing a radar reflectivity of 22dbZ near the ground. In the same region in the run with α_R=0, the rain evaporates almost totally, producing a radar reflectivity of only 10dbZ near the ground. The radar observations of this shower show that in regions where the reflectivity is around 20 25dbZ just below the melting layer (at 1500m) the reflectivity is only 2dbZ lower at the ground below, due to evaporation of rain into the dry boundary layer air. This agrees very well with the radar profile diagnosed from the simulation with α_R=2.5.

The use of a non-zero shape parameter had other effects on the evolution of the modelled convective cells. With α_R=2.5 the peak rate that rain accretes liquid water is 10% less than for α_R=0, even though the fall velocity is 16% greater, (figures calculated assuming q_R=0.2g kg^{-1} and q_L=1g kg ^{1}). The effect of the

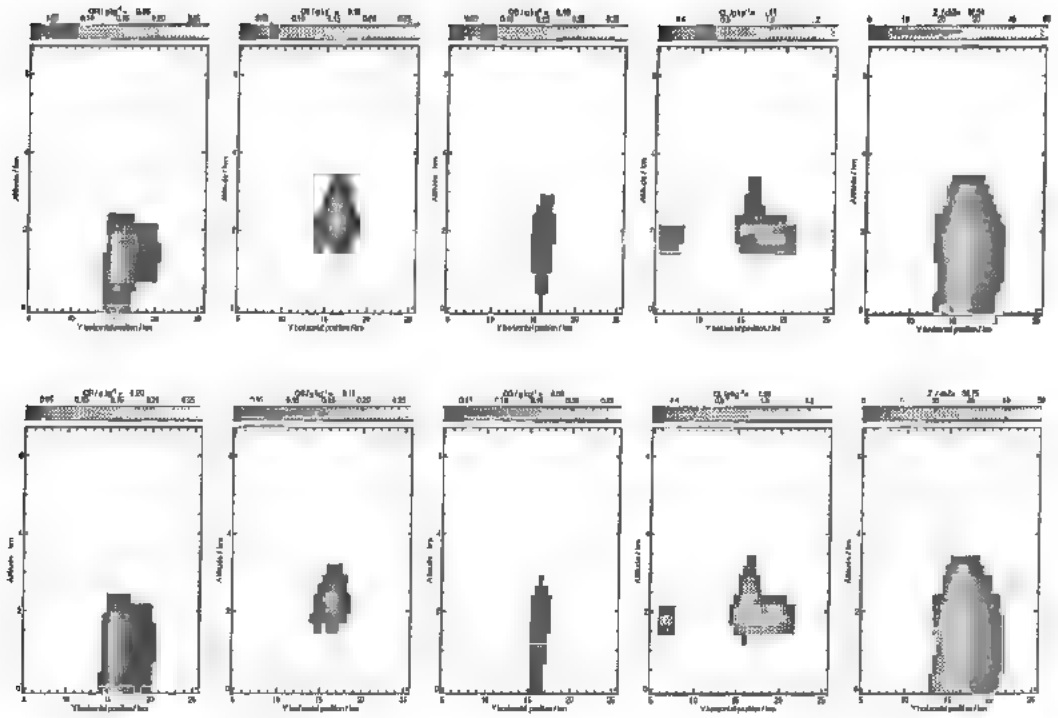

Figure 7: *Vertical cross sections showing rain, snow, graupel and liquid cloud mixing ratios and radar reflectivity from a simulation with α_R=0 (top row) an a simulation with α_R=2.5 (bottom row)*

reduced residence time of rain in the cloud and the reduced rate of accretion is that 30% less rain had reached the ground after 200 minutes of simulation in the run with α_R=2.5. Also more liquid and ice cloud were present in the α_R=2.5 run, but less snow, graupel and rain.

Using a value of α_R=2.5 improved the vertical profile of rain below cloud base, which could be validated by comparing diagnosed radar reflectivity from the model with observed reflectivity. But this change in the shape parameter also caused a large reduction in the precipitation efficiency, which is less easily vali dated by observations, as the intensity of the showers observed on that day varied temporally and spatially.

7 Discussion

This work raises a number of points for discussion relevant to the parametrization of rain, and other hydrometeors, as described below.

7.1 Value of the shape parameter

The explicitly modelled drop size spectra evolutions suggest that a non-zero value of α allows bulk parametrization schemes to model the size spectra more accurately in the evaporating region. This is a simple alteration that can improve the representation of evaporation in GCMs that at present assume an exponential size distribution of rain (Gregory 1995)

This parameter is completely independent of the mass mixing ratio and the mean diameter so the rain drop spectrum is defined by three parameters *ie.* three independent observables are required to obtain the values of the parameters. Goddard and Cherry (1984) obtained α_r=5 by considering distrometer and radar measurments. Ulbrich and Atlas (1984) obtained α_r=2 from analysis of distrometer derived Z and Z_{DR}, and rainfall rate. Another cloud modeller, Ferrier (1993) uses a value of 2.5 based on optical spectrometer measurements by Willis (1984). Wilson (1995) obtained values of α_r between 2 and 10 averaging 5, using radar observations of differential doppler velocity, Z_{DR} and Z.

7.2 Parametrization of initialisation, breakup and coalescence of rain

The 1-D evaporation model described here does not include a parameterization of the break–up and coalescence processes or any of the in–cloud drop growth mechanisms. The effect of break up and coalescence of rain is to maintain an equilibrium size spectrum of roughly exponential shape with intercept parameter of $8 \times 10^6 m^{-4}$. Brown (1994) describes this equilibrium state in detail. The justification of ignoring these processes is that the effect of evaporation on the size spectra occurs on shorter a time scale than the breakup/coalescence time scale at the relatively low rain rates examined here; the time for this steady state spectrum to occur is around 300 seconds (based on the mean time for a 1mm

diameter raindrop to collide with another drop when the rain rate is 8mm/hour) which is longer than the time for a 1mm diameter drop to completely evaporate. In simulations of rain with higher rainrates, the representation of break up and coalescence would become more important as these processes would occur on a shorter time scale.

In a more comprehensive 1–D rain model, break up and coalescence should be parametrized. More importantly in 3–D cloud models the initiation of rain drop number concentration also needs to be parametrized. This is made difficult in the Large Eddy Model by the highly simplified representation of liquid cloud water (a constant number concentration is assumed). It would be difficult to accurately represent the rain initiation without better representation of liquid cloud.

7.3 Use of double–moment representation for hydrometeors other than rain

For a number of reasons the use of a double–moment scheme for snow and graupel is even more desirable than using it for rain. The intercept parameter (and hence the mean diameter for a given mass mixing ratio) varies more for graupel and snow than for rain. This is because breakup limits the number of large rain drops, whereas snow and graupel particles can grow far larger than the largest rain drops. Rutledge and Hobbs (1983) use a value of graupel intercept parameter of 4×10^{4}m ^{4} whereas Swann and Brown (1996) use a value based on observations of $4\times10^{6}\mathrm{m}^{-4}$. Similarly for snow, the intercept parameter is found to vary by two orders of magnitude as shown by observations described by Lo and Passarelli (1981).

In the LEM a parametrization already exists for the creation of pristine ice crystals by deposition onto natural ice nuclei, collision freezing of liquid drops with aerosols and secondary ice multiplication process, (Swann 1994). With the number concentration of ice crystals described accurately, it is possible to model the initiation of the number concentrations of snow and graupel using parametrizations based on the assumptions used in single–moment schemes, such as those described by Lin et al (1983) and Rutledge and Hobbs (1983).

In the double–moment scheme, the calculation of the depletion of rain drop number concentration due to evaporation is based on the assumption that the mean drop size is unaffected by this process. Results using this assumption agree well

with the explicit scheme. The process of evaporation is similar to the processes of sublimation and melting of precipitating ice particles in that it is proportional to the heat transfer from the particles' surface, so the assumption that the mean particle sizes are unaffected by these processes should be used for schemes using double-moment representation for ice particles.

8 Conclusions

The 1-D simulations have revealed a number shortcomings and advantages in using the two types of bulk schemes and in the value of the shape parameter. The following points have arisen from this work with significance to the parametrization of rain in CRMs and mesoscale models.

- The single–moment scheme over-estimates the evaporation because it predicts that the mean rain drop radius reduces considerably when rain undergoes evaporation, when the explicit model shows this not to be the case. By increasing the value of the shape parameter from α 0 (*ie* an exponential size spectrum) to $\alpha = 2.5$, this problem is reduced considerably, as demonstrated by the 3–D simulation in section 6. This alteration can be made to microphysics schemes without incurring any increase in the computation required by the microphysics parametrization.

- The double–moment scheme is able to model the large drops falling faster and reaching the ground first when rainfall commences suddenly (an observation easily made when standing outside before the start of a shower). The scheme tends to exaggerate this vertical spreading out of drop sizes, especially when assuming an exponential drop spectrum ($\alpha - 0$), because the size spectrum is artificially broadened. This aspect is improved by assuming a sharper distribution of drop sizes with the shape parameter set to $\alpha - 2.5$.

- For modeling the below–cloud evaporation layer, the double–moment scheme was more accurate than the single–moment scheme (whatever value of the shape parameter was used). This conclusion is based on the single–moment scheme consistently overestimating the amount of evaporation. It should be noted that the double–moment scheme is more computationally expensive (an additional variable typically increases both the required computer time and memory by 10%) , and also that the parametrization of the initialisation of rain number concentration and breakup and coalescence has not been addressed here.

References

Brown, P. S., 1994: Vertical Variation of the Steady–State Drop Spectrum in a One–Dimensional Rain Shaft. *J. Atmos. Sci.* **51,** 2075–2085

Brown, P. R. A. and H. Swann, 1996: The observational validation of a 3-d numerical cloud model used for the development of convective cloud parametrization schemes. (submitted to Q. J. R. Meteorol. Soc.).

Byers, H. R., 1965: Elements of cloud physics. *University of Chicago press,* 191pp.

Clough, S. A. and R. A. A. Franks, 1989: Evaporation of Frontal and other Stratiform precipitation. *Q. J. R. Met. Soc.* **117,** 1057–1080.

Kessler, E., 1969: On the distribution and continuity of water substance. *Meteor. Monogr.* **No.32,** Amer. Meteor. Soc.

Lin, Y- L., R. D. Farley, and H. Orville, 1983: Bulk parametrization of the snow field in a cloud model. *J. Climate. Appl. Met.*, **22,** 1065–1092.

Lo, K. K. and R. E. Passarelli, Jr. 1981: The Growth of Snow in Winter Storms: An Airborne Observation Study. *J. Climate and Applied Met.* **22,** 1065 1092.

Ferrier, B. S., 1993: A Double–Moment Multiple–Phase Four–Class Bulk Ice Scheme. Part1: Description. *J. Atmos. Sci.* **51,** 249–280.

Flatau, P. J., G. J. Tripoli , J. Verlinde and W. R. Cotton, 1989: The SCU-RAMS Cloud microphysics module general theory and code documentation. *Colorado State University, Paper No.* **451.**

Goddard, J. W. F. and S. M. Cherry, 1984: Quantitative Precipitation Measurments with Dual Linear Polarization Radar. *Preprints, 22nd International Conference on Radar Meteorolgy, Amer. Meteor. Soc., Boston,* 352–357.

Gregory, D., 1995. The Consistent Treatment of the Evaporation of Rain and Snow foe Use in Large–Scale Models *Monthly Weather Review* **123,** 2716–2732.

Thorpe, A. D. and Mason, B. J., 1966: The evaporation of ice spheres and ice crystals. *Brit. J. Appl. Phys.* **17,** 541–556.

Willis, P. T., 1984: Functional fits to some observed drop size distributions and parametrization of rain. *J. Atmos. Sci.*, **41,** 1648–1661

Wilson, D. R., 1995: Advanced Polarization and Doppler Radar Techniques to Study Precipitation Microphysics. *PhD. Thesis, Reading University.*

Uplinger, W. G., 1981: A new formula for raindrop terminal velocity. *Proc. 20th Conf. on Radar Meteorology,* Boston, American. Meteor. Soc., 389–391

Ulbrich, C. W. and D. Atlas, 1984:Assessment of the contribution of differential polarization to improved rainfall measurements *Radio Science* **19** 49–57.

CURRENT JCMM INTERNAL REPORTS

This series of JCMM Internal Reports, initiated in 1993, contains unpublished reports and also versions of articles submitted for publication. The complete set of Internal Reports is available from the National Meteorology Library on loan, if required.

1. **Research Strategy and Programme.**
   K A Browning et al
   January 1993

2. **The GEWEX Cloud System Study (GCSS).**
   GEWEX Cloud System Science Team
   January 1993

3. **Evolution of a mesoscale upper tropospheric vorticity maximum and comma cloud from a cloud-free two-dimensional potential vorticity anomaly.**
   K A Browning
   January 1993

4. **The Global Energy and Water Cycle**
   K A Browning
   July 1993

5. **Structure of a midlatitude cyclone before occlusion.**
   K A Browning and N Roberts
   July 1993

6. **Developments in Systems and Tools for Weather Forecasting.**
   K A Browning and G Szejwach
   July 1993

7. **Diagnostic study of a narrow cold frontal rainband and severe winds associated with a stratospheric intrusion.**
   K A Browning and R Reynolds
   August 1993

8. **Survey of perceived priority issues in the parametrizations of cloud-related processes in GCMs.**
   K A Browning
   September 1993

9. **The Effect of Rain on Longwave Radiation.**
   I Dharssi
   September 1993

10. **Cloud Microphysical Processes - A Description of the Parametrization used in the Large Eddy Model.**
H Swann
July 1994

11. **An Appreciation of the Meteorological Research of Ernst Kleinschmidt.**
A J Thorpe
May 1992

12. **Potential Vorticity of Flow Along the Alps.**
A J Thorpe, H Volkert and Dietrich Heimann
August 1992

13. **The Representation of Fronts.**
A J Thorpe
January 1993

14. **A Parametrization Scheme for Symmetric Instability: Tests for an Idealised Flow.**
C S Chan and A J Thorpe
February 1993

15. **The Fronts 92 Experiment: a Quicklook Atlas.**
Edited by T D Hewson
November 1993

16. **Frontal wave stability during moist deformation frontogenesis. Part 1. Linear wave dynamics**
C H Bishop and A J Thorpe
May 1993

17. **Frontal wave stability during moist deformation frontogenesis. Part 2. The suppression of non-linear wave development.**
C H Bishop and A J Thorpe
May 1993

18. **Gravity waves in sheared ducts.**
S Monserrat and A J Thorpe
October 1993

19. **Potential Vorticity and the Electrostatics Analogy: Quasi-Geostrophic Theory.**
C Bishop and A J Thorpe
November 1993

20. **Recent Advances in the Measurement of Precipitation by Radar.**
A J Illingworth
April 1993

21. **Micro-Physique et Givrage. Cloud Microphysics and Aircraft Icing.**
A J Illingworth
May 1993

22. **Differential Phase Measurements of Precipitation.**
M Blackman and A J Illingworth
May 1993

23. **Estimation of Effective Radius of Cloud Particles from the Radar Reflectivity.**
N I Fox and A J Illingworth
May 1993

24. **A Simple Method of Dopplerising a Pulsed Magnetron Radar.**
L Hua, A J Illingworth and J Eastment
November 1993

25. **Radiation and Polar Lows.**
George C Craig
February 1994

26. **Collected preprints submitted to International Symposium on the Life Cycles of Extratropical Cyclones; Bergen, Norway, 27 June - 1 July 1994**
April 1994

27. **Convective Frontogenesis**
Douglas J Parker and Alan J Thorpe
April 1994

28. **Improved Measurement Of The Ice Water Content In Cirrus Using A Total Water Evaporator**
Philip R A Brown and Peter N Francis
April 1994

29. **Mesoscale Effects of a Dry Intrusion within a Vigorous Cyclone**
K A Browning and B W Golding
April 1994

30. **GEWEX Cloud System Study, Science Plan**
May 1994

31. **Parametrization of Momentum Transport by Convectively Generated Gravity Waves**
R Kershaw
February 1995

32. **Mesoscale Modelling Newsletter, No. 5**
May 1994

33. **Observations of the mesoscale sub-structure in the cold air of a developing frontal cyclone**
K A Browning, S A Clough, C S A Davitt, N M Roberts and T D Hewson
May 1994

34. **Longwave Radiative Forcing of a Simulated Tropical Squall Line**
Imtiaz Dharssi
July 1994

35. **On the nature of the convective circulations at a kata-cold front**
K A Browning
September 1994

36. **Collected preprints of papers submitted to the COST-75 International Seminar on Advanced Weather Radar Systems, Brussels, 20-23 September 1994**
November 1994

37. **Use of satellite imagery to diagnose events leading to frontal thunderstorms: Parts I and II of a case study**
K A Browning and N M Roberts
November 1994

38. **The role of spaceborne millimetre-wave radar in the global monitoring of ice cloud**
P R A Brown, A J Illingworth, A J Heymsfield, G M McFarquhar, K A Browning and M Gosset
December 1994

39. **Potential Vorticity Inversion**
Michal Ziemianski
October 1994

40. **Theory of mature tropical cyclones; A comparison between Kleinschmidt (1951) and Emanual (1986)**
Suzanne L Gray
December 1994

41. **Dispersion and removal of pollutants during the passage of an atmospheric frontal system**
N R Gimson
December 1994

42. **The role of snow sublimation in frontogenesis**
D J Parker and A J Thorpe
December 1994

43. **Potential vorticity and the electrostatics Analogy: Ertel-Rossby formulation**
A J Thorpe and C H Bishop
December 1994

44. **Mesoscale aspects of extratropical cyclones: an observational perspective**
K A Browning
January 1995

45. **A Polar Low Outbreak: Evolution and Mesoscale Structures**
T D Hewson, G C Craig and C Claud
February 1995

46. **Generation of near-surface gusts by deep convection**
K Nakamura and R Kershaw
April 1995

47. **Attribution concepts applied to the omega equation**
S A Clough, C S A Davitt and A J Thorpe
June 1995

48 **Parametrization of mixed-phase cloud and precipitation**
Susan P Ballard and M Gerard Hutchinson
June 1995

49 **Short-range forecasting of stratocumulus: Initialization V Prediction**
Susan P Ballard, Simon D Jackson and B Macpherson
June 1995

50 **Contributions of the JCMM/Dept of Meteorology Radar Group to the 27th AMS Radar Meteorology Conference, Vail October 1995**
June 1995

51 **Cold pools in shear**
Douglas J Parker
September 1995

52 **High-resolution analysis of frontal fracture**
K A Browning, S P Ballard and C S A Davitt
September 1995

53 **The Albedo of Broken Cloud Fields: Calculations using a modified two stream radiation code**
Imtiaz Dharssi and Roy Kershaw
October 1995

54 **Parametrization of momentum transport by convection. I: Theory and cloud modelling results**
R Kershaw and D Gregory
November 1995

55 **Variation of frontal structure along a cold front**
K A Browning and N M Roberts
November 1995

56 **Secondary Frontal Waves**
Douglas Parker
December 1995

57 **Objective Fronts**
T D Hewson
March 1996

58 **Mesoscale analysis of the activation of a cold front during cyclogenesis**
K A Browning, N M Roberts and A J Illingworth
June 1996 *Not yet produced*

59 **Investigation of different representations of rain in a 1-d evaporation model**
H Swann
May 1996

Met Office Joint Centre for Mesoscale Meteorology Department of Meteorology
University of Reading PO Box 243 Reading RG6 6BB United Kingdom
Tel: +44 (0)118 931 8425 Fax: +44 (0)118 931 8791
www.metoffice.com